RSC Advances

ROYAL SOCIETY OF CHEMISTRY

www.rsc.org/advances

Dual application of Pd nanoparticles supported on mesoporous silica SBA-15 and MSU-2: Supported catalysts for C−C coupling reactions and cytotoxic agents against human cancer cell lines

Adriana Balbín,[a] Francesco Gaballo,[a] Jesús Ceballos-Torres,[a] Sanjiv Prashar,[a] Mariano Fajardo,[a] Goran N. Kaluđerović[b,*] and Santiago Gómez-Ruiz[a,*]

[a] *Departamento de Biología y Geología, Física y Química Inorgánica, Escuela Superior de Ciencias Experimentales y Tecnología, Universidad Rey Juan Carlos, Calle Tulipán s/n, E-28933, Móstoles (Madrid), Spain.*

[b] *Department of Bioorganic Chemistry, Leibniz Institute of Plant Biochemistry, Weinberg 3, D-06120 Halle (Saale), Germany*

ABSTRACT

Two different mesoporous silica-based materials (SBA-15 and MSU-2) have been treated under mild conditions with different quantities of [$PdCl_2$(cod)] (cod = 1,5-cyclooctadiene) to promote the formation of supported palladium nanoparticles (materials of the type SBA-15-Pd and MSU-2-Pd). The synthesized materials have been characterized by different techniques observing that the palladium nanoparticles remain impregnated in the silica. The catalytic activity of the hybrid Pd-silica materials has been tested in Suzuki-Miyaura C–C coupling reactions observing moderate conversion rates in the reactions of 3-bromoanisole with 4-carboxyphenylboronic acid and 2-bromopyridine with 4-carboxyphenylboronic acid. In addition, the synthesized materials showed a good degree of recyclability, being catalytically active in five consecutive catalytic tests. Finally, in order to evaluate the cytotoxicity of the synthesized materials, *in vitro* tests against five different human cancer cell lines have been carried out, observing high cytotoxic activities of the hybrid systems comparable if not somewhat higher to other systems based on metal complexes supported on mesoporous silicas described previously in the literature. To the best of our knowledge the cytotoxic study reported here represents the first evaluation of the anticancer action of supported palladium nanoparticles in human cancer cells.

KEYWORDS

Pd nanoparticles; SBA-15; MSU-2; Suzuki-Miyaura C–C coupling reactions; biological activity

* Corresponding authors:
Dr. Santiago Gómez-Ruiz (santiago.gomez@urjc.es)
Dr. Goran N. Kaluđerović (goran.kaluderovic@ipb-halle.de)

1. INTRODUCTION

Metal nanoparticles have attracted much attention over the last decade in a variety of applications including sensors, non-linear optics, medical dressings and catalysis.[1,2,3,4] The supporting material on which these nanoparticles are synthesized has also received significant scrutiny in the literature.[1] The choice of solid supports in the synthesis of impregnated metal nanoparticles is very wide, ranging from organic polymers[5] to various transition metal oxides,[6] and including mesoporous silicas[1] and microporous zeolites.[7] However, the most important factors to consider when choosing the support material are its thermal and chemical stability under the reaction conditions and its ability for the facile dispersion and accessibility of the metal nanoparticles (this is generally achieved with materials with high surface areas (> 100 m^2/g) and mesoporous structures (pore size > 2 nm)).[1] In this context, mesoporous silicas have been considered to be very good supports for metal nanoparticles. Mesoporous silicas were discovered in the early 1990s by scientists at Mobil Oil Company and by Kuroda and co-workers, in part as a response for the need of extending the applications of zeolites.[8] These interesting materials offer many of the features expected from an ideal support: a very large surface area (> 600 m^2/g), a narrow pore distribution (2–50 nm), high thermal and chemical stability, ready availability and easy chemical modification on the surface by anchoring catalytically active species. Due to their properties, mesoporous silicas are actively being exploited as supports in catalysis. The presence of functional groups and active species on the surface (thiol groups, organic ligands, metal nanoparticles, etc.) has a great influence on the recyclability of the catalyst, on its activity and on the agglomeration of the nanoparticles.[1]

The physical properties and catalytic activity of supported catalysts are highly dependent on the support, methods of preparation and type and method of preparation of the noble metal particles.[9] The incorporation and position of palladium nanoparticles in the final hybrid material and the maximum effective loading of metal nanoparticles are aspects that must be considered in the nanoparticle preparation. Finally, the control of size and morphology of the nanoparticles and how to maintain it during the catalytic reaction are two main problems that remain unsolved. In addition, the presence of certain functional groups on the surface of the supports may have an important role regarding these aspects, as well as other such as catalytic activity or controlling the phenomenon of particle agglomeration.[9]

Currently, supported catalysts are prepared in two ways: directly during surface synthesis or by post-synthesis treatment of the surface with a palladium precursor. The post-synthetic methods are normally based on impregnation of a Pd precursor (e.g. palladium acetate) followed by its reduction with various reducing agents (ethanol, $NaBH_4$, H_2, hydrazine),[1,2,9] ion exchange with metal precursors,[10] adsorption of molecular cluster precursors,[11] immobilization of metal

complexes[12] or photocatalytic reduction.[13] The method used for the synthesis of the nanoparticles on the support, inside the pores as well as on its external surface, affects their distribution and size in a decisive manner. For example, it has been found that if the synthesis of Pd nanoparticles occurs simultaneously to the synthesis of the silica support MCM-41, the nanoparticles remain anchored to the outer surface, while if they are introduced through a post-synthesis treatment they can be incorporated within the mesoporous structure of MCM-41.[14] In addition, several reports have been published using SBA-15 mesoporous materials as scaffolds for the preparation of palladium nanoparticles[15,16,17] with similar results to those described for MCM-41, however, nothing is known about the use of other mesoporous silica with disordered pores such as MSU-2, in the preparation of such hybrid systems.

All the cited methods are fast and simple, but when the catalyst is reused, the activity decreases dramatically due to its structure collapsing.[18] Additionally, the kinetics of the metal reduction process, in most cases, is not easily controllable, nor green nor simple to carry out; so that the product also needs to be thoroughly washed and conditioned in order to remove the excess of reducing agent. This has led to a high number of reports concerning improvements in the preparation methods of metal nanoparticles, and recently, some research groups have employed glucose as an environmentally benign reducing agent to prepare well-dispersed metal nanoparticles with an excellent catalytic activity in C−C cross coupling reactions and a very easy recyclability.[2] Additionally, many other groups have used a previous functionalization of the mesoporous silica with amino or thiol groups for an easier reduction of the metal salt and *in situ* formation of the metal nanoparticle.[19,20,21,22]

Thus, metal nanoparticles supported on mesoporous silicas have shown interesting catalytic properties, however, at the present time only very limited reports have analyzed the cytotoxicity of supported palladium nanoparticles or free palladium nanoparticles.[23,24,25,26] From other cytotoxic studies with metal oxide nanoparticles one can envisage that nanoparticles influence the cytotoxic effects according to their particle size, surface area and the type and concentration of metal ions released into the medium, being the latter the most important effect on the cytotoxicity.[27] Furthermore, it is known that the cytotoxic nature is greater for soluble nanoparticles.[27] The development of nanoparticles-based anticancer drugs has become important in the world of biomedicine, since they act only in cancer cells and have fewer side effects. The mechanisms by which these nanoparticles exhibit anticancer activity are not fully understood.[27] However, it is known that the key to understanding the nanoparticle cytotoxicity is their small size, lower than that of a cell, which allows them to penetrate the biological structures, altering their normal function. In addition, the nanoparticles side effects on human health, beyond the chemistry, size, shape, charge, agglomeration state and electromagnetic

properties, depend on individual factors such as genetic and existing disease,[27] although further studies in this topic must be carried out in the future.

Thus, bearing in mind the interest in the catalytic and biological properties of metal nanoparticles, in this paper we report the synthesis, characterization and catalytic properties of palladium nanoparticles supported on SBA-15 and MSU-2 which represents the first study of the preparation of palladium nanoparticles using a mesoporous silica with a non-ordered pore distribution (MSU-2). In addition, the synthetic method described here for the preparation of the hybrid systems does not need a previous functionalization of the mesoporous silica with amino or thiol groups, but a simple reduction of an organometallic salt of Pd such as [$PdCl_2$(cod)] in a single step. The synthesized materials showed moderate conversions and a good degree of recyclability in C-C coupling Suzuki-Miyaura reactions.

In addition, we herein report the preliminary evaluation of the *in vitro* cytotoxic activity of the hybrid materials against four different human cancer cell lines which shows a dose-dependent activity with M_{50} values between 110±20 and 553±13 μg/mL. This represents the first report describing the cytotoxic properties of supported palladium nanoparticles. These studies should be useful as a starting point for subsequent investigations of palladium nanoparticles with biological properties.

2. EXPERIMENTAL

2.1. General conditions

All manipulations were performed under dry nitrogen gas using standard Schlenk techniques and dry box. Solvents were distilled from the appropriate drying agents and degassed before use. Tetraethylorthosilicate (TEOS) 98% (MW = 208.33, d = 0.934 g/mL), poly(ethylene glycol)-block-poly(propylene glycol)-blockpoly(ethylene glycol) (Pluronic 123, M_{av} = 5800; d = 1.019 g/mL), NaF (extra pure) and Tergitol® NP-9 (MW = 616.82), all from Sigma-Aldrich, were used as purchased, without further purification. Water (resistance 18.2 MΩcm) used in the preparation of materials was obtained from a Millipore Milli-Q-System (Billerica, MA, USA).

2.2 General remarks on the characterization of the materials

X-ray diffraction (XRD) pattern of the silicas were obtained on a Philips Diffractometer model PW3040/00 X'Pert MPD/MRD at 45 KV and 40 mA, using a wavelength Cu Kα (λ = 1.5418 Å). Pd wt % determination by X-ray fluorescence were carried out with a X-ray fluorescence

spectrophotometer Philips MagiX with an X-ray source of 1kW and a Rh anode using a helium atmosphere. The quantification method is capable of analyzing from 0.0001% to 100% Pd. N_2 gas adsorption-desorption isotherms were performed using a Micromeritics ASAP 2020 analyzer. Scanning electron micrographs and morphological analysis were carried out on a XL30 ESEM Philips with an energy dispersive spectrometry system (EDS). The samples were treated with a sputtering method with the following parameters: Sputter time 100 s, Sputter current 30 mA film thickness 20 nm using a Sputter coater BAL-TEC SCD 005. Conventional transmission electron microscopy (TEM) was carried out on a TECNAI 20 Philips, operating at 200 kV.

2.3 Preparation of non-functionalized materials

2.3.1. Preparation of SBA-15

The synthesis of SBA-15 was carried out using the experimental procedure reported by Zhao *et al.*[28] In a typical synthesis, TEOS 98% aqueous solution (102 g, 0.480 mol) was added dropwise to a stirring solution containing the Pluronic 123 surfactant (48.4 g), 360 mL of Milli-Q water and 1342 mL of HCl 2 M at 35 °C and 1000 rpm. After the TEOS addition, the reaction was stirred (1000 rpm) at 35 °C for 20 h. During this time, a white solid was formed in the reaction solution. Stirring was then stopped and the temperature was increased to 80 °C and maintained for 24 h, in order to complete the ageing process.

Afterwards, the solution was filtered under vacuum and the resulting white solid was abundantly washed with Milli-Q water, in order to eliminate soluble impurities and the remaining surfactant. After washing, a drying process (at 100 ºC during 6 h) and a subsequent calcination process (during 24 h at 500°C) were carried out in a muffle oven. After the calcination process, 29.17 g of fine white powder of SBA-15 was obtained.

2.3.2. Preparation of MSU-2

The synthesis of MSU-2 was carried out using the experimental procedure previously reported.[29] In a typical synthesis, Tergitol® (78.135 g, 0.103 mol) was added in a two-necked flask containing 1562.5 mL of stirring Milli-Q water. After the complete dissolution of Tergitol®, TEOS (52.0 g, 0.250 mol) was added dropwise to the solution. After 30 min, stirring was stopped and the solution was left to age for 20 h; slowly forming a white suspension. After the ageing process, stirring was set at 800 rpm and 26 mL of NaF 0.24 M solution was added dropwise to the flask. Afterwards, the temperature was raised to 55 °C and the solution was stirred for an additional 48 h. Subsequently, the solution was filtered using a gooch filter

connected to a vacuum line; the white solid was abundantly washed with Milli-Q water, in order to eliminate all the soluble impurities and the remaining surfactant. After washing, a drying process (at 100 ºC during 6 h) and a subsequent calcination process (during 20 h at 600 °C) were carried out in a muffle oven. After calcination, 15.08 g of a fine white powder of MSU-2 was obtained.

2.4. Preparation of the hybrid materials SBA-15-Pd-X or MSU-2-Pd-X

2.4.1. Synthesis of Pd nanoparticles precursor: [$PdCl_2$(cod)]

$PdCl_2$ (3.05 g, 17.2 mmol) was dissolved in 8 mL of concentrated HCl. The cooled solution was diluted with 250 mL of absolute ethanol and filtered through a filter paper; the residue and filter paper were then washed with 40 mL of ethanol. After this step, 1,5-cyclooctadiene (5.0 mL, 40.7 mmol) was added to the resulting solution under stirring, the solution turned from brown to deep yellow and the solid product precipitated immediately. The reaction was stirred for an additional 15 min and then filtered and the yellow solid product was washed with diethylether (3 × 20 mL). The final product was dried under vacuum overnight giving 4.80 g (16.8 mmol) of [$PdCl_2$(cod)] as a yellow solid (yield: 98%).

2.4.2. Mesoporous silica activation

Before the functionalization reactions, the mesoporous silica-based materials SBA-15 and MSU-2 need to be activated. The activation consists in the dehydration and elimination of the physisorbed solvents on the hydroxyl functional groups present on the surface by the treatment of the corresponding surface under vacuum conditions for 24 h at 150 °C.

2.4.3. Synthesis of materials SBA-15-Pd-X and MSU-2-Pd-X

Two different hybrid materials have been synthesized by functionalization of two types of mesoporous silicas, SBA-15 and MSU-2 through the reduction of the palladium precursor [$PdCl_2$(cod)]. Table 1 shows the quantity of palladium complex and mesoporous silicas employed in each reaction.

The general procedure carried out for the preparation of the hybrid materials was as follows: in a dry box, the corresponding amount of the mesoporous silica and [$PdCl_2$(cod)] were added to a Schlenk tube and dried under vacuum for 1 h at room temperature. Subsequently, 30 mL of tetrahydrofurane (THF) were added under an inert atmosphere. The reaction mixture was then heated at 80 °C and stirred for 48 h. The reaction conditions were determined after several syntheses at different temperatures, reaction times and solvents, showing that the greater

efficacy was obtained using THF as solvent, at 80 °C and reaction time of 48 h. Subsequently, the hybrid material was filtered and washed several times with solvents of increasing volatility (2 × 50 mL each), namely THF, toluene, hexane and diethylether. Finally, the material was dried under vacuum for 12 hours to remove all solvent trace. This procedure was repeated for each initial amount of palladium and for all the studied materials (SBA-15 and MSU-2).

2.5. Catalytic tests

2.5.1. Preliminary tests

Catalytic tests were focused on two reactions:

1) Reaction between 3-bromoanisole and 4-carboxyphenylboronic acid (Scheme 1)
2) Reaction between 2-bromopyridine and 4-carboxyphenylboronic acid (Scheme 2)

The reactions were performed under identical conditions, in order to facilitate a subsequent analysis of the results. Thus, the limiting reagent was the halide derivative, the molar ratio between the boronic acid and the halide was 1.2 to 0.8, the molar ratio between the base (K_2CO_3) and the halide was 2 to 1 and the amount of catalyst was always 50 mg. The experimental procedure was identical for both reactions, using the corresponding halide in each case. Degassed solvents and a nitrogen atmosphere were used in the reaction to achieve higher final conversions.[22]

In a typical catalytic reaction a three-neck flask was filled with boronic acid (0.2 g, 1.2 mmol), K_2CO_3 (0.22 g, 1.6 mmol) and Pd catalyst and three vacuum/N_2 cycles (10 min/1 min) under stirring were applied to remove oxygen from the reaction atmosphere. In parallel, the solvent (DMF/H_2O 95/5, 10 mL) and the aryl halide were mixed under nitrogen in a Schlenk tube, bubbling N_2 inside the solution for 15 min to eliminate dissolved oxygen. Subsequently, this mixture was transferred under $N_2$to the three-neck flask with the solid mixture. The suspension was then heated to the corresponding temperature (using a condenser in the case of refluxing conditions) and stirred for 24 h. After this time, the solution was cooled to room temperature and the solvent was removed under vacuum.

The catalytic activity of the synthesized materials in the Suzuki-Miyaura coupling reactions has been compared to the activity of a homogeneous Pd catalyst, [$Pd(PPh_3)_4$] using 1% Pd.

2.5.1.1. Purification of the catalytic products

The purification of the product was achieved using a chromatographic column, charged with silica gel and the suitable eluent to separate the reaction product. The latter was chosen on the basis of tests carried out on thin layer chromatography (TLC).

For reaction 1 (3-bromoanisole + 4-carboxyphenylboronic acid), dichloromethane/toluene (9/1) was used as the eluent solution. Solvent was removed from the solution containing the product with a rotavapor and the light yellow solid obtained was dried overnight at 60 °C under vacuum. ^{1}H-NMR (400 MHz, D_2O, 25 °C): δ = 4.60 (s, 3H, -OCH_3), 6.84, 7.07, 7.14 and 7.27 (m, 1H each, H of anisole ring), 7.75 and 7.52 (d, 2H each, H of 4-carboxyphenyl ring), COOH (not observed).

For reaction 2 (2-bromopyridine + 4-carboxyphenylboronic acid) acetonitrile/water (7/3) was used as the eluent solution. Solvent was removed from the solution containing the product with a rotavapor and the orange solid obtained was dried at 60 °C under vacuum overnight. ^{1}H-NMR (400 MHz, d_6-DMSO, 25 °C): δ = 7.29 (m, 1H, Pyr), 7.86 (m, 2H, Pyr), 7.93 (m, 1H, Pyr), 7.78 and 7.69 (d, 2H each, H of 4-carboxyphenyl ring), 10.00 (br, 1H, COOH).

2.5.1.2. Quantification of the conversion rate

The technique employed to quantitatively analyze the conversion of 3-bromoanisole and to identify the reaction product was gas chromatography (GC) with FID detector (Varian CP-3370) using a 15 m CP-SIL-8 column provided by Scharlau. The kinetics or the conversion of the different reactions was determined by following the variation of the concentration of 3-bromoanisole in solution. To follow the changes of the halide concentration, an internal standard compound (1-octanol) was used. Comparing the areas relating to the signals of the halo compound and the internal standard, the concentration of the halide can be determined with accuracy. The chosen internal standard was 1-octanol (100 ppm), an inert compound with respect to reagents and products and that has a retention time different from the others compounds. The solution samples to be analyzed were diluted in the ratio 1:50 in order to adjust the concentration of reactants and products to the range of linearity of the calibration curve. The calibration curve was prepared using concentration of halide in the range 0-500 ppm for both reactions. The temperature conditions were: injector temperature: 240 °C, detector temperature: 250 °C, oven temperature program 130 °C (10 min); from 130 °C to 210 °C (with a ramp of 20 °C/min) and 210 °C (10 min). Operating under these conditions the retention times of the chemical species in solution were, DMF: 3.5 min, 1-octanol: 6.5 min, 2-bromopyridine: 7.8 min, 3-bromoanisole: 12.0 min, 4-carboxyphenylboronic acid: 16.7 min, product of the first reaction: 20.0 min, product of the second reaction 19.6 min. The tests were carried out in triplicate, (the reported results are the average of those obtained). For an example of a chromatogram of the reaction mixture see Figure S1 of the Supplementary Material.

2.5.2. Catalytic study of the influence of Pd quantity

Additional catalytic tests have been carried out to study the conversion of the 3-bromoanisole in reaction 1 (3-bromoanisole + 4-carboxyphenylboronic acid) using different amounts of catalyst. The conversion studies were carried out using 15 mg and 5 mg of each of the following catalysts: **SBA-15-Pd-50** and **MSU-2-Pd-15**. Conversion experiments were performed in a single-neck Schlenk tube. Solution samples were collected and analyzed at the beginning and at the end of the reaction time. For these tests, the experimental procedure was as follows: to a Schlenk tube, 4-carboxyphenylboronic acid (9.95 mg, 0.06 mmol), K_2CO_3 (11.05 mg, 0.08 mmol) and Pd catalyst (15 mg or 5 mg) were added and three vacuum/N_2 cycles (10 minutes/1 minute) applied under stirring to eliminate oxygen. Subsequently a solution of 3-bromoanisole (7.5 mg, 0.04 mmol) in DMF/H_2O 95/5, (15 mL, with a previous N_2 bubbling of 10 minutes) was added to the mixture. The suspension was then heated to 70 °C and stirred for 48 hours. 1:10 dilutions of the samples were analyzed by GC.

2.5.3. Study of the catalyst recyclability

Additional catalytic tests were carried out to determine the loss of activity of the catalysts after several catalytic cycles. Recyclability tests were carried out using similar experimental procedure but tested in up to five catalytic cycles in a row using the catalysts **SBA-15-Pd-50** and **MSU-2-Pd-15**. Thus, the reactions were performed on a larger scale, under the same experimental conditions. The tests started from a higher amount of catalyst (1.0 g) in order to be able to carry out five catalytic cycles. After each catalytic cycle, the catalyst was filtered and washed with water (2 × 100 mL) and diethylether (2 × 30 mL). The final amounts of reactants used in the different recyclability tests are shown in Table S1 of the Supplementary material.

2.6. Cytotoxicity in vitro studies

2.6.1. Drug preparation

Stock suspensions of the palladium-functionalized materials were prepared in PBS (phosphate buffer) at a proportion of 20 mg/mL and diluted by nutrient medium to various working concentrations. In all cases, nutrient medium was RPMI-1640 (PAA Laboratories) supplemented with 10% fetal bovine serum (Biochrom AG) and 1% penicillin/streptomycin (PAA Laboratories).

2.6.2. Cell culture

The cell lines used in the present study, 8505 C (anaplasic thyroid cancer), A253 (head and neck cancer), A549 (lung carcinoma), A2780 (ovarian cancer) and DLD-1 (colon cancer) were kindly provided by Dr. Thomas Mueller, Department of Hematology/Oncology, Martin Luther University of Halle-Wittenberg, Halle (Saale), Germany. Cultures were maintained as monolayer in RPMI-1640 (PAA Laboratories, Pasching, Germany) supplemented with 10% heat inactivated fetal bovine serum (Biochrom AG, Berlin, Germany) and penicillin/streptomycin (PAA Laboratories) at 37 °C in a humidified atmosphere of 5% (v/v) CO_2.

2.6.3. Cytotoxicity assay

The cytotoxic activity of the materials was evaluated using the sulforhodamine-B (SRB, Sigma Aldrich) microculture colorimetric assay.[30] Cancer cells were seeded into 96-well plates and kept under incubation for 24 h. Afterwards, the cells were treated with various suspensions of increasing concentration of the materials to be analyzed.

The percentage of surviving cells was determined 96 h after the beginning of drug exposure. After 96 h treatment, the supernatant medium from the 96 well plates was eliminated and the cells were fixed with a 10% solution of trichloroacetic acid (TCA). After fixation, the cells were washed in a strip washer. The washing was carried out four times with water using alternate dispensing and aspiration procedures.

The plates were then dyed with 100 µL of 0.4% SRB for about 45 min. After dying, the plates were again washed to remove the dye with 1% acetic acid and dried to air overnight. 100 µL of 10 mM tris-hydroxymethylaminoethane (TRIS) was added to each well of the plate and absorbance was measured at 570 nm using a 96-well plate reader (Tecan Spectra, Crailsheim, Germany). The M_{50} value was estimated from the dose-response curves and was defined as the quantity (in µg/mL) of the material at which 50% cell inhibition was observed.

3. RESULTS AND DISCUSSION

3.1. Synthesis and characterization of supported palladium nanoparticles

3.1.1. Synthesis of supported palladium nanoparticles

Two silica-based mesoporous materials (SBA-15[28] and MSU-2[29]) were synthesized according to reported procedures and were then treated with increasing amounts of [$PdCl_2$(cod)] in THF during 48 hours to give hybrid materials which consisted of the corresponding silica support impregnated with palladium nanoparticles. Under the proposed reaction conditions [$PdCl_2$(cod)] is reduced to form palladium nanoparticles that remain adsorbed in the material. The mechanism of the reaction appears to proceed via the reduction of the palladium salt by THF which, together with the hydroxyl groups at the surface of the materials, acts as a reducing agent. Once palladium nanoparticles are formed, they accumulate in the pores of the corresponding materials. When the reaction is conducted at longer time periods the palladium nanoparticles remain impregnated in the external surface of the silica support.

3.1.2. Characterization by X-ray Fluorescence

X-ray fluorescence analysis was carried out to determine the quantity of embedded palladium in the hybrid materials. A detailed study of the loading curves using different amounts of palladium precursor (1, 2, 5, 10, 20 and 50% wt. Pd) was performed in order to determine the amount of metal lost during the synthesis, and thus, observe if there is a maximum saturation level in the functionalization.

For SBA-15, the maximum percentage of incorporated palladium was 12.8% wt.; which was obtained when starting from theoretical 50 % wt. Pd. The data from all the experiments showed a linear trend in the studied loading range (see Figure S2 of Supplementary Material). However, it seems unlikely that this linearity persists with higher percentages of initial palladium, even though; a maximum of saturation was not observed in the studied range (see Figure S2 and Table 1).

For MSU-2, the maximum percentage of incorporated palladium was 4.46% wt. which was obtained when starting from a theoretical 20 % wt. Pd. In this case, MSU-2 showed a non linear trend for the incorporation of palladium (see Figure S3 of Supplementary Material and Table 1), although, again, no saturation was found in the studied range. Compared to SBA-15, the amount of incorporated palladium was generally lower in MSU-2, probably due to the smaller average pore diameter of MSU-2.

3.1.3. Characterization by N_2 adsorption-desorption

All the studied materials were characterized by N_2 adsorption-desorption isotherms (BET method), which allowed the specific surface area of the materials, the average pore diameter and the pore volume to be determined. Figure 1 illustrates the adsorption-desorption isotherms of SBA-15 and MSU-2. According to the IUPAC classification, SBA-15 presents a typical type IV isotherm with a H1 hysteresis loop, which features a two-dimensional *P6mm* structure formed by open cylindrical mesopores,[31] while MSU-2 shows a type IV isotherm with a type H4 hysteresis loop typical of some disordered mesoporous systems.[31] Comparing the textural properties of silica-based materials, one can easily see that MSU-2 shows a greater specific surface area, a smaller pore diameter and a greater pore volume than SBA-15. All the obtained parameters are in the range of reported mesoporous silica.[28,29] In addition, a narrow pore size distribution was observed for SBA-15 and MSU-2 (see Figure S4 of Supplementary Material). The narrow and defined peaks are typical of a homogeneous pore diameter distribution.

For the Pd-functionalized hybrid materials, all the N_2 adsorption-desorption isotherms were very similar to those of their parent materials. As expected, all the Pd-functionalized materials exhibited slightly lower surface areas and lower average pore volume compared to their parent material, due to Pd deposition within the pores and/or on the surface of the materials. This probably leads to a slight blocking of the pore in detriment of the surface area and pore volume (See Table 2). This phenomenon was especially notable when increasing the Pd loading in samples **SBA-15-Pd-50** and **MSU-2-Pd-20**. On the other hand, pore average diameter did not remarkably change after formation of the palladium nanoparticles.

3.1.4. Characterization by X-ray Diffraction

SBA-15, MSU-2 and their corresponding Pd-functionalized analogues were characterized by low angle X-ray diffraction. The low angle XRD patterns of unmodified SBA-15 and MSU-2 are shown in Figure 2. Both materials exhibit a well resolved pattern, with two diffraction peaks at 0.95° (100) and 1.89° (110) for SBA-15, and at 1.90° (100) and 3.46° (110) for MSU-2. The observed XDR patterns correspond to a mesoscopic order attributed to mesoporous materials. Observing the diffraction peaks of the two materials it is clear that SBA-15 presents a more ordered structure than MSU-2, since it presents lower peak broadening. In these structures, the d_{100} spacing, assigned to the pore-to-pore centre correlation distance for each plane, was 92.20 and 46.43 Å for SBA-15 and MSU-2, respectively.

The XDR reflections observed for the functionalized materials are similar to their non-functionalized analogues, with relatively small differences in the peak broadening and a slight decrease of their intensity due to a relatively small partial blocking of the dispersion centres as a consequence of the functionalization. This fact provides evidence that part of the functionalization process occurs inside the mesopore channels, since the attachment of metal

nanoparticles or organic functional groups here normally reduces the scattering power of the mesoporous silica walls. Analyzing the data of the interplanar distances of all silica-based mesoporous materials, it is possible to calculate the average wall thickness of the studied materials, using the following equation:

$$\text{Wall thickness} = \frac{2d_{100}}{\sqrt{3}} - \text{BJH average pore diameter} \quad (1)$$

The average wall thickness is 38.5 and 15.2 Å for unmodified SBA-15 and MSU-2, respectively. The wall thickness slightly increases after functionalization in the case of SBA-15 (with values from 38.6 to 40.2 Å), while it is apparently constant in the case of MSU-2 functionalized materials (with values from 14.6 to 15.9 Å). These results indicate that part of the Pd-nanoparticles may be located inside the pores of the corresponding materials.

For all the Pd-functionalized hybrid materials high angle X-ray diffractograms were recorded in order to observe the peaks associated to palladium nanoparticles (Figure 3). Comparing the obtained diffractograms with others reported in the literature for Pd nanoparticles,[2,32] the assignation of the corresponding Miller indices was possible. Thus, the most intense peaks at 2θ of 39.3, 45.4 and 67.5° were assigned to the (111), (200) and (220) planes, respectively, while the secondary peaks in intensity, at 80.3 and 84.6°, were assigned to the (311) and (222) planes, respectively.

3.1.5. Characterization by SEM

All the synthesized materials have been characterized by Scanning Electronic Microscopy (SEM), in order to observe the morphology of the studied surfaces. There were significant differences between the non-functionalized and the hybrid materials. The SBA-15-based materials (Figure 4a) showed uniform morphology of nanostructured rods (similar particle size of 695±77 nm long and 459±41 nm width, for particle size distribution see Figure S5 of Supplementary Material), while MSU-2 (Figure 4b) and its analogues show a similar spherical particle shape with similar mean diameter of 782±162 nm (for particle size distribution see Figure S6 of Supplementary Material). In solid state, both types of silica-based materials have a tendency to form clusters of aggregated particles.

3.1.6. Characterization by TEM

All the non-functionalized materials have been characterized by Transmission Electronic Microscopy (TEM). Figure 5a and 5b shows the transmission electron micrograph (TEM)

images of SBA-15 material which presents a highly ordered structure, with a hexagonal ordered porous parallel channels. In the case of MSU-2 materials (Figure 5c and 5d), the particles lack regular channel packaging order but exhibit a 3D worm-hole porous framework.

For the Pd-functionalized materials (Figure 6), one can easily detect the palladium nanoparticles as black dots either inside the pore of the mesoporous particles or impregnated on the external surface of the support. All hybrid materials show spherical palladium nanoparticles with diameters of 29±9 nm for SBA-15-based materials (Figure 6a) and 28±5 nm for MSU-2-based materials (Figure 6b) (for the particle size distribution see Figures S7 and S8 of the Supplementary Material). In all cases, the larger palladium particles appear to be clusters of very small nanoparticles.

Reaction time has an influence on the morphology and location of palladium nanoparticles. The reaction of the formation of palladium nanoparticles was monitored by TEM. When using SBA-15, one can observe that after just 6 hours of reaction (Figure 7a) the main part of the palladium nanoparticles are located inside the pores showing a spherical or slightly elongated shape, where they grew following the directions of the channels. However, after 48 hours of reaction, all the Pd-nanoparticles are impregnated on the outer surface of the mesoporous matrix (Figure 6a).

On the other hand, after just 6 hours of reaction, the MSU-2-based materials did not show the palladium nanoparticles inside the non-regular pores of the mesoporous material (Figure 7b), but always impregnated onto the mesoporous particle surface, observing almost no changes after 48 h of reaction (Figure 6b).

As observed in the corresponding images (Figure 6), palladium nanoparticles show a very high tendency to aggregate on the surface of the mesoporous materials (especially at higher loadings) resulting in a less homogeneous dispersion of the metal. The highly ordered structure of SBA-15 seems to promote a better incorporation of palladium nanoparticles within the mesoporous structure, as was indicated by the greater decrease in the specific surface area and pore volume, compared to MSU-2 (see data of N_2 adsorption-desorption analyses in Table 2). However, applying longer reaction times to the non-ordered starting material MSU-2, leads to a better distribution of the Pd nanoparticles.

3.2. Catalytic tests

3.2.1. Preliminary catalytic tests in Suzuki-Miyaura C-C coupling reactions

The catalytic activity of the Pd based materials in S-M reactions was tested in two coupling reactions involving a boronic acid with two different aromatic halides. For each reaction a test

using a homogeneous commercial catalyst ([$Pd(PPh_3)_4$] was carried out in order to compare the catalytic activity of the studied materials.

All the catalytic tests were carried out under previously reported experimental conditions,[22] using a DMF/H_2O (95/5) mixture as solvent, K_2CO_3 as base and measuring the final conversion 24 hours after starting the reaction.

Table 3 shows the results obtained in the preliminary tests, for the reaction between 3-bromoanisole and 4-carboxyphenylboronic acid (Scheme 1) and Table 4 shows the results obtained in the catalytic reaction between 2-bromopyridine and 4-carboxyphenylboronic acid (Scheme 2).

It seems that the temperature has an influence on the conversion, observing, in all cases, higher catalytic activities when the temperature decreases from 110 to 70 °C. This phenomenon suggests that temperatures higher than 70 °C may lead to some changes in the physical structure either of the catalysts or of the reactants which may affect the catalytic activity.

In this context, material **SBA-15-Pd-50** was analyzed by TEM after the reaction at 110 ºC observing the formation of relatively big agglomerates of Pd nanoparticles (see Figure S9 of supplementary material). The agglomeration is normally favoured with an increase of the temperature and is associated with lower activity, thus giving a plausible explication for the catalytic results obtained. In addition, the higher catalytic activity of the reference compound ([$Pd(PPh_3)_4$] at 70 ºC compared to that of 110 ºC may be explained by a possible deactivation of the catalyst due to the fact that at higher temperatures the formation of palladium nanoparticles may also occur and interfere with the catalytic reaction.[33]

A subsequent study of the halide conversion at different time periods in both reactions showed two different types of behavior. In catalytic test #9 between 3-bromoanisole and 4-carboxyphenylboronic acid, there is a rapid decrease of the concentration of the halide after the first 4 h followed by a slower decrease until the end of reaction time with a final conversion of 3-bromoanisole of 84% (see Figure S10 of the Supplementary Material). In the case of catalytic test #19 between 2-bromopyridine and 4-carboxyphenylboronic acid the concentration of the halide decreases more slowly and progressively during the reaction time, and does not seem to reach a minimum after 24 hours (with a final conversion of 2-bromopyridine of 40 %) (see Figure S11 of the Supplementary Material).

The differences in the conversion of both reactions seems to be justified by the fact that the *meta*-substituted arylbromides react faster than *ortho*-substituted derivatives (as is the case of 2-bromopyridine) due to steric factors. In addition, the inductive effect (-I) exerted by the methoxy group, which removes electron density, weakens the C−Br bond, increases its

reactivity. The reactivity of 2-bromopyridine seems to be lowered also by the conjugative effect, due to the electron pair present at the nitrogen atom of the aromatic ring.

On analysis of the efficiency of the catalytic reactions regarding the halide conversion per mg of Pd in the mixture one can see that the most effective catalysts are those with a lower Pd content. It seems that the Pd nanoparticles are more accessible in the case of those materials with a lower load, maybe due to a higher degree of agglomeration in materials with high palladium content. In addition, very similar efficiency was achieved for both MSU-2 or SBA-15-based materials (Tables 3 and 4).

In order to show the versatility of the synthesized hybrid materials in C-C coupling reactions, **SBA-15-Pd-50** was also used as catalyst in the S-M reaction of 4-vinylboronic acid and 3-bromoanisole, observing a reasonable degree of halide conversion (41±1%), which is lower to that described for the reaction with 4-carboxyphenylboronic acid using 15 mg (for further details see the Supplementary Material). In addition, **SBA-15-Pd-20** was tested as catalyst in the Sonogashira reaction of iodobenzene and phenylacetylene and a modest yield of 36% of diphenylacetylene was obtained (for further details see the Supplementary Material).

3.2.2. Study of the effect of Pd quantity in Suzuki-Miyaura C-C coupling reactions

Taking into account all the above results, we decided to study the catalytic activity of the materials focusing exclusively on the reaction between 3-bromoanisole and 4-carboxyphenylboronic acid due to its higher conversion rates and selecting the optimum reaction conditions for these catalytic tests based on the previous results. These experiments were carried out at 70 °C, in a DMF/H_2O (95/5) solvent mixture and using K_2CO_3 as the base. A reaction time of 48 h was chosen because after this time there was no further significant decrease in the concentration of 3-bromoanisole (see Figure S6 of the Supplementary Material). The catalysts used for these tests were **SBA-15-Pd-50** and **MSU-2-Pd-15**.

The results of the tests using the studied materials as catalysts in the reaction between 3-bromoanisole and 4-carboxyphenylboronic acid are summarized in Table 5. Higher conversions were obtained using higher amounts of catalyst. This phenomenon may be due to influence of the Pd content which increases the halide conversion in this type of catalytic system.

From these experiments using different quantities of catalyst, one observes, in both cases (SBA-15 and MSU-2), a higher catalytic efficiency (halide conversion per mg of Pd) using 15 mg of catalyst, than when using 5 mg of material. In addition, a slightly higher efficiency was achieved in these tests when using MSU-2-based materials compared to SBA-15 (Table 5). This probably arises from a better distribution of Pd nanoparticles in **MSU-2-Pd-15** compared to that of the more Pd-loaded catalyst **SBA-15-Pd-50** (see Section 3.2.1).

3.2.3. Preliminary study of the recyclability of the catalysts

Catalyst recycling was investigated under the same reaction conditions used in the conversion tests. Since the recovery of the catalyst in small quantities is very difficult, we designed experiments using higher amounts of catalyst but maintaining the molar ratio of all the reactants and solvents. The catalysts used for these tests were **SBA-15-Pd-50** and **MSU-2-Pd-15**.

In the recycling tests a substantial loss of activity of the catalysts was observed after the first recycle test. A loss of activity of around 36% (from halide conversions of 63 to 39%) for **SBA-15-Pd-50** and or ca. 35% (from halide conversions of 39 to 26%) for **MSU-2-Pd-15** indicates the partial deactivation of the catalysts or leaching of the palladium nanoparticles after the first cycle. However, in the second and subsequent catalytic cycles the activity remained almost the same and did not show significant changes (Figure 8). These results suggest a loss of activity by an initial leaching or deactivation of the supported catalyst that may affect only the non-impregnated palladium nanoparticles, which, because of their low size, are lost after the first catalytic cycle and subsequent filtration process. However, this does not happen after the second catalytic cycle because all the remaining Pd-nanoparticles are impregnated on the silica materials and do not leach after washing or filtration treatments. With this in mind, a TEM analysis of the materials used in the recyclability tests was carried out after the first catalytic cycle observing the formation of Pd nanoparticles agglomerates which are usually located on the external surface of the mesoporous materials (see Figure S12 of the Supplementary Material). This phenomenon may explain the lose of catalytic activity after the first catalytic cycle. For the second and subsequent catalytic cycles, there is no significant growth of the Pd palladium nanoparticle agglomerates which remain impregnated on the mesoporous silica Higher aggregates are probably not formed due to their lower mobility in suspension resulting from the larger particle size.

For the MSU-2 materials (non-ordered mesoporous silica), the decrease in the catalytic activity for the second and subsequent cycles is slightly lower to that of SBA-15. This might be due to a higher degree of dispersion of the nanoparticles in the MSU-2-based materials (with the same Pd load) and a lower tendency for the formation of agglomerates with respect to SBA-15, indicating a slight positive influence of the use of non-ordered mesoporous silica such as MSU-2.

In summary, these results show a good degree of stability of the studied catalysts in C-C coupling reactions although somewhat lower than some other similar systems described in the literature for the Heck reaction,[34] and comparable to those described for Suzuki-Miyaura C-C coupling reactions.[35,36]

3.3. Preliminary cytotoxicity tests

Mesoporous silica-based materials functionalized with metal complexes have demonstrated very high cytotoxic activity and high potential for their application in chemotherapy.[37–42] Bearing this in mind, a preliminary study of the cytotoxic activity of the Pd-functionalized materials **SBA-15-Pd-50** and **MSU-2-Pd-15**, has been carried out in order to gain new insights on the cytotoxic properties of supported palladium nanoparticles and their potential as anticancer drugs.

The materials have been analyzed in *in vitro* tests against anaplasic thyroid carcinoma (8505C), head and neck tumour (A253), lung carcinoma (A549) and colon carcinoma (DLD-1) cell lines. Cytotoxicity values, expressed as M_{50} values (the amount of material required to inhibit normal cell growth of the studied cell population by 50%), are given in Table 6. The studied materials **SBA-15-Pd-50** and **MSU-2-Pd-15** show a dose-dependent cytotoxicity (Figure 9) against all the studied cancer cells. Taking into account that the unmodified mesoporous silica-based materials have not shown cytotoxic activity in previous studies reported by our group,[37,38,39,40,41,42] it seems reasonable to assume that palladium nanoparticles play a crucial role in the cytotoxic action.

In addition, the fact that **SBA-15-Pd-50** (with a Pd amount of 12.80% wt. and having M_{50} values from 110±16 to 239±20 μg/mL) shows higher cytotoxic activity in all the studied cancer cell lines than **MSU-2-Pd-15** (with a Pd amount of 2.18% wt. with M_{50} values from 241±18 to 553±13 μg/mL), indicates again the influence of the palladium nanoparticles and that palladium content is essential to give a substantial increase in the cytotoxic activity.

The comparison of the cytotoxic activity of the studied materials with other mesoporous silica-based materials functionalized with metal complexes, shows the M_{50} values of **SBA-15-Pd-50** are one of the lowest of all the studied systems, indicating their relatively high cytotoxic activity. In this context, only the recently reported tin-[41] and titanocene-functionalized materials[42] have shown higher cytotoxic activity in cancer cell lines.

Interestingly, both materials reported here, **SBA-15-Pd-50** and **MSU-2-Pd-15**, have shown a lower cytotoxicity against A549 cells compared with the other tested cell lines. This phenomenon led us to believe that there might be some differences in the mechanism associated to the cell death promoted by these hybrid materials in the cancer cell lines. However, caution must be taken when analyzing the tendencies in the cytotoxic nature of these materials as many factors such as, the quantity of material used, palladium content, studied cell type and mesoporous silica type, come into play.

4. CONCLUSIONS

Supported palladium nanoparticles have been synthesized using SBA-15 and for the first time using MSU-2 as supports and [$PdCl_2$(cod)] as a palladium precursor in a simple reaction which does not need the use of functionalized silica-based nanostructured materials. The functionalization reactions show different tendencies for the incorporation of the metal nanoparticles depending on the supporting material with a maximum load of Pd of 12.80% wt. on SBA-15 and 4.46% wt. on MSU-2, observing that systems with a disordered arrangement of the pores (MSU-2) gave lower Pd conversion to nanoparticles. The hybrid materials have been used as catalysts for the Suzuki-Miyaura (SM) coupling reaction between 3-bromoanisole and 4-carboxyphenylboronic acid and the reaction between 2-bromopyridine and 4-carboxyphenylboronic acid. Maintaining the same reaction conditions, a higher catalytic activity was observed at 70 °C compared to 110 °C. This is probably due to the formation of bigger agglomerates of palladium nanoparticles at higher temperatures which partially deactivate the hybrid catalysts, as was deduced from the TEM analysis of the resulting materials after the catalytic reaction. The reaction between 3-bromoanisole and 4-carboxyphenylboronic acid catalyzed by the hybrid materials and the reference catalyst [$Pd(PPh_3)_4$] is faster with both heterogeneous and homogeneous catalysts (needing only 24 h for the maximum conversion) than that of 2-bromopyridine and 4-carboxyphenylboronic acid (which needs around 48 h) and this may be due either to steric and/or electronic factors. In addition, the results show that the most effective catalysts are those with a lower Pd content. It seems that the Pd nanoparticles are more accessible in the case of those materials with a lower load, that have a better distribution of the palladium nanoparticles and/or a higher degree of agglomeration in materials with respect to materials with high palladium content. However, very similar efficiency was achieved for both MSU-2- and SBA-15-based materials in the studied catalytic tests. Additionally, in the reaction between 3-bromoanisole and 4-carboxyphenylboronic acid catalyzed by **SBA-15-Pd-50** or **MSU-2-Pd-15**, conversion of the halide compound was quantified using 15 mg or 5 mg of fresh catalyst observing that the highest conversions were obtained when using 15 mg indicating the influence of the quantity of palladium on the final catalytic activity, although a slightly higher catalytic efficiency was observed when using 15 mg. A recyclability study using **SBA-15-Pd-50** and **MSU-2-Pd-15** in up to six catalytic cycles was carried out observing that the conversion of the halide is reduced after the first cycle, however, it remains nearly constant for the other five cycles indicating a reasonable degree of recyclability of the studied materials. This phenomenon is probably due to the significant agglomeration of Pd-particles after the first catalytic cycle. This is not as dramatic in the second and subsequent catalytic cycles because the

bigger Pd nanoparticles remain impregnated on the mesoporous silica without forming higher aggregates due to their lower mobility in suspension associated to their higher particle size.

Hybrid materials **SBA-15-Pd-50** and **MSU-2-Pd-15** have been tested *in vitro* against human cancer cells observing a dose dependent cytotoxicity in all the studied cancer cell lines and a higher cytotoxic effect of **SBA-15-Pd-50** compared to **MSU-2-Pd-15**. According to our experiments it seems that the cytotoxic nature of these materials depends on the quantity of material used, palladium content, studied cell type and mesoporous silica type. To the best of our knowledge, this is the first report about the cytotoxic activity of supported palladium nanoparticles and further study on the mechanistic aspects of the cell death induction promoted by these materials needs to be carried out in order to determine if these palladium nanoparticle functionalized materials are potential candidates for therapeutic treatments.

5. ACKNOWLEDGEMENTS

We gratefully acknowledge financial support from the Ministerio de Economía y Competitividad, Spain (Grant no. CTQ2012-30762). A. Benedetti and D. Pérez are gratefully acknowledged for helpful discussion.

6. REFERENCES

1 R. J. White, R. Luque, V. L. Budarin, J. H. Clark and D. J. Macquarrie, *Chem. Soc. Rev.* 2009, **38**, 481–494.

2 V. Budarin, J. H. Clark, R. Luque, J. Macquarrie, J. Robin and R. White, *Green Chem.* 2008, **10**, 382–387.

3 V. Mody, R. Siwale, A. Singh, and H. R. Mody, *J. Pharm. Bioallied Sci.* 2010, **2**, 282–289.

4 Nanoparticles and Catalysis. Edited by Didier Astruc, WILEY-VCH Verlag GmbH & Co. KGaA, Weinheim (2008).

5 W. A. Lopes and H. M. Jaeger, *Nature*, 2001, **414**, 735–738.

6 J. S. Aaron, J. Oh, T. A. Larson, S. Kumar, T. E. Milner and K. V. Sokolov, *Optics Express*, 2006, **14**, 12930–12943.

7 A. B. Laursen, K. T. Højholt, L. F. Lundegaard, S. B. Simonsen, S. Helveg, F. Schüth, M. Paul, J.-D. Grunwaldt, S. Kegnæs, C. H. Christensen and K. Egeblad, *Angew. Chem. Int. Ed.* 2010, **49**, 3504–3507.

8 I. Slowing, J. L. Vivero-Escoto, B. G. Trewyn and V. S.-Y. Lin, *J. Mater. Chem.* 2010, **20**, 7924–7937.

9 V. Barau, A. Budarin, R. Caragheorgheopol, D. J. Luque, A. Macquarrie, V. S. Prelle, M. Teodorescu and A. Zaharescu, *Catal. Lett.* 2008, **124**, 204–214.

10 J. He, I. Ichinose, T. Kunitake and A. Nakao, *Langmuir*, 2002, **18**, 10005–10010.

11 L. Guczi, A. Beck, A. Horváth and D. Horváth, *Top. Catal.* 2002, **19**, 157–163.

12 H. Ye, R. W. J. Scott and R. M. Crooks, *Langmuir*, 2004, **20**, 2915–2920.

13 A. Troupis, E. Gkika, A. Hiskia and E. Papaconstantinou, *Compt. Rendus Chim.* 2006, **9**, 851–857.

14 Á. Mastalir, B. Rác, Z. Király and Á. Molnár, *J. Molec. Catal. A: Chem.* 2007, **264**, 170–178.

15 K. Liu, Z. X. Chen, Z. Q. Hou, Y. Y. Wang and L. Y. Dai, *Catal. Lett.* 2014, **144**, 935–942

16 P. Li, H. Liu, Y. Yu, C. Y. Cao and W. G. Song, *Chem. Asian J.* 2013, **8**, 2459–2465.

17 C. M. A. Parlett, D. W. Bruce, N. S. Hondow, M. A. Newton, MA A. F. Lee and K. Wilson *ChemCatChem* 2013, **5**, 939–950.

18 I. Yuranov, P. Moeckli, E. Suvorova, P. Buffat, L. Kiwi-Minsker and A. Renkena, *J. Mol. Catal. A: Chem.* 2003, **192**, 239–251.

19 S. MacQuarrie, B. Nohair, J. H. Horton, S. Kaliaguine and C. M. Crudden *J. Phys. Chem. C* 2010, **114**, 57–64.

20 C. Y. Ma, B. J. Dou, J. J. Li, J. Cheng, Q. Hu, Z. P. Hao and S. Z. Qiao, *Appl. Catal. B: Environm.* 2009, **92**, 202–208.

21 R. Xing, Y. Liu, H. Wu, X. Li, M. He and P. Wu, *Chem. Commun.*, 2008, 6297–6299.

22 M. Trilla, G. Borja, R. Pleixats, M. W. C. Man, C. Bied, and J. J. E. Moreau, *Adv. Synth. Catal.* 2008, **350**, 2566–2574.

23 A. Speranza, K. Leopold, M. Maier, A. R. Taddei and V. Scoccianti, *Environm. Pollution*, 2010, **158**, 873–882.

24 C. P. Adams, K. A. Walker, S. O. Obare and K. M. Docherty *PLoS ONE* 2014, **9**, e85981.

25 D. De Stefano, R. Carnuccio and M. C. Maiuri, *J. Drug Deliv.* 2012, Article ID 167896.

26 C. Petrarca, E. Clemente, L. Di Giampaolo, R. Mariani-Costantini, K. Leopold, R. Schindl, L. V. Lotti, R. Mangifesta, E. Sabbioni, Q. Niu, G. Bernardini and M. Di Gioacchino, *J. Immunol. Res.* 2014, Article ID 295092.

27 M. Horie, K. Fujita, H. Kato and S. Endoh, *Metallomics* 2012, **4**, 350–360.

28 D. Zhao, Q. Huo, J. Feng, B. Chmelka, G. Stucky, *J. Am. Chem. Soc.*, 1998, **120**, 6024–6036.

29 D. Pérez-Quintanilla, A. Sánchez, I. Hierro, M. Fajardo, I. Sierra, *J. Nanosci. Nanotech.*, 2009, **9**, 4901–4909.

30 P. Skehan, R. Storeng, D. Scudiero, A. Monks, J. McMahon, D. Vistica, J. T. Warren, H. Bokesch, S. Kenney and M. R. Boyd, *J. Nati. Cancer Inst.* 1990, **82**, 1107–1112.

31 K. S. W. Sing, D. H. Everett, R. A. W. Haul, L. Moscou, R. A. Pierotti, J. Rouquerol and T. Siemieniewska, *Pure & Appl. Chem.* 1985, **57**, 603–619.

32 S. Navaladian, B. Viswanathan, T. K. Varadarajan and R. P. Viswanath, *Nanoscale Res. Lett.* 2009, **4**, 181–186.

33 R. Molina, S. Gómez-Ruiz, F. Montilla, A. Salinas-Castillo, S. Fernández-Arroyo, M. M. Ramos, V. Micol and R. Mallavia , *Macromolecules* 2009, **42**, 5471–5477.

34 M. Arpad, *Chem. Rev.* 2011, **111**, 2251–2320.

35 G. H. Zhang, P. Y. Wang and X. F. Wei, *Catal. Lett.* 2013, **143**, 1188–1194.

36 B. Basu and S. Paul, *Appl. Organomet. Chem.* 2013, **27**, 588–594.

37 D. Perez-Quintanilla, S. Gómez-Ruiz, Ž. Žizak, I. Sierra, S. Prashar, I. del Hierro, M. Fajardo, Z. D. Juranić and G. N. Kaluđerović, *Chem. Eur. J.* 2010, **12**, 5588–5597.

38 G. N. Kaluđerović, D. Perez-Quintanilla, I. Sierra, S. Prashar, I. del Hierro, Ž. Žizak, Z. D. Juranić, M. Fajardo and S. Gómez-Ruiz, *J. Mater. Chem.* 2010, **20**, 806–814.

39 G. N. Kaluđerović, D. Perez-Quintanilla, Ž. Žizak, Z. D. Juranić and S. Gómez-Ruiz, *Dalton Trans.* 2010, **39**, 2597–2608.

40 A. García-Peñas, S. Gómez-Ruiz, D. Perez-Quintanilla, R. Paschke, I. Sierra, S. Prashar, I del Hierro and G. N. Kaluđerović, *J. Inorg. Biochem.* 2012, **106**, 100–110.

41 M. Z. Bulatović, D. Maksimović-Ivanić, C. Bensing, S. Gómez-Ruiz, D. Steinborn, H. Schmidt, M. Mojić, A. Korać, I. Golić, D. Pérez-Quintanilla, M. Momčilović, S. Mijatović and G. N. Kaluđerović, *Angew. Chem. Int. Ed.* 2014, **53**, 5982–5987.

42 J. Ceballos-Torres, P. Virag, M. Cenariu, S. Prashar, M. Fajardo, E. Fischer-Fodor, S. Gómez-Ruiz, *Chem. Eur J*, 2014, **20**, 10811–10828.

Figures, Schemes and Tables

Figure 1. Nitrogen adsorption-desorption isotherms of SBA-15 and MSU-2

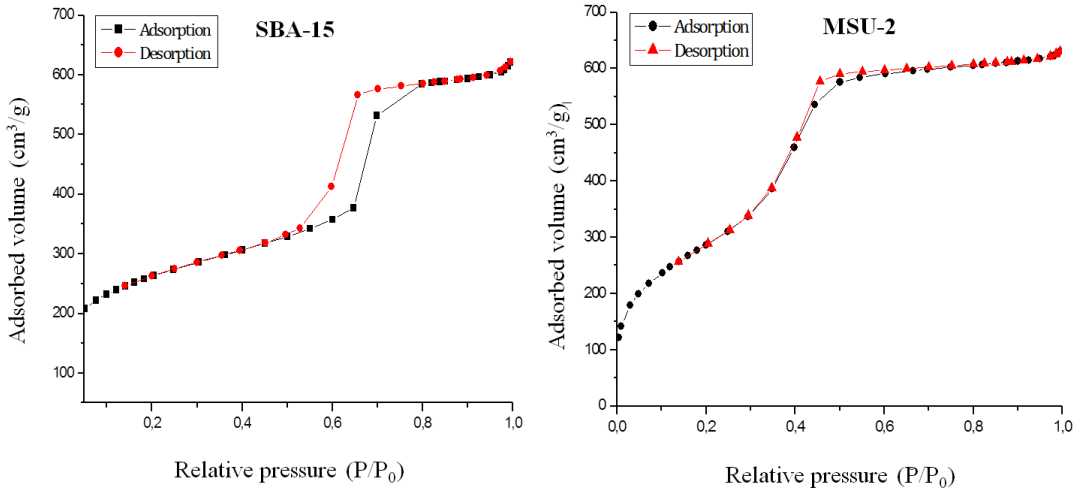

Figure 2. Low angle X-ray diffractograms of SBA-15 and MSU-2

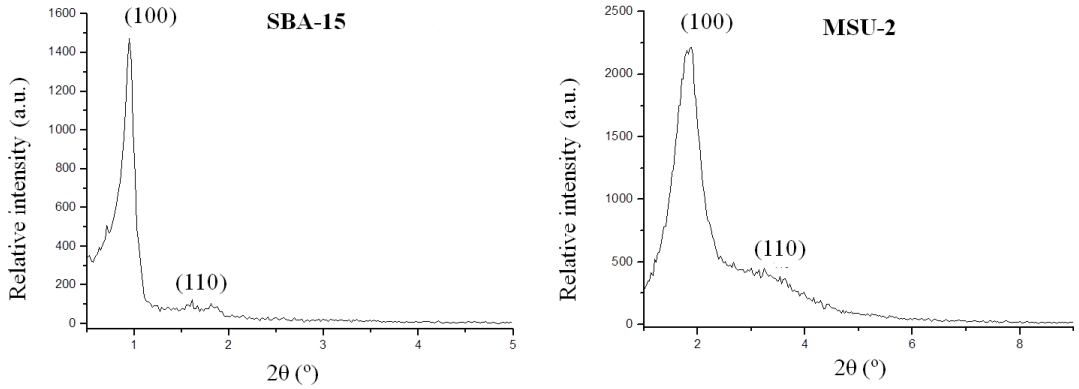

Figure 3. High angle X-ray diffractogram of SBA-15-Pd-50

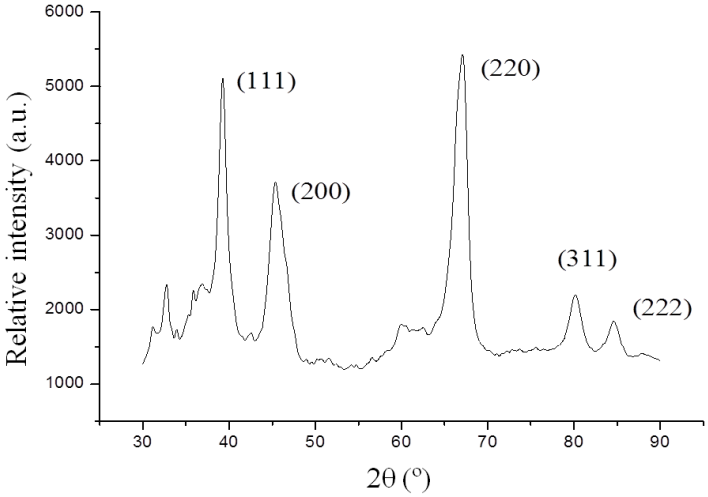

Figure 4. SEM images of (a) SBA-15 and (b) MSU-2

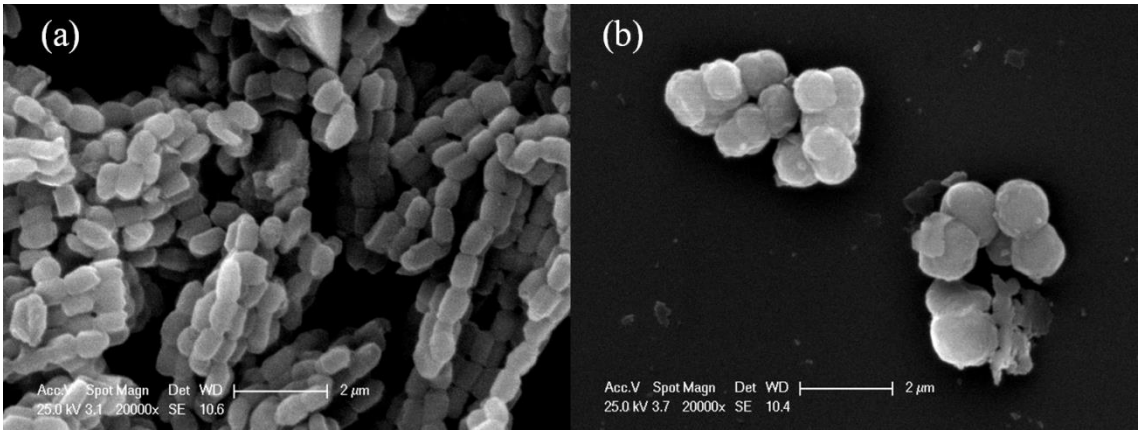

Figure 5. TEM images of (a) and (b) SBA-15 and (c) and (d) MSU-2

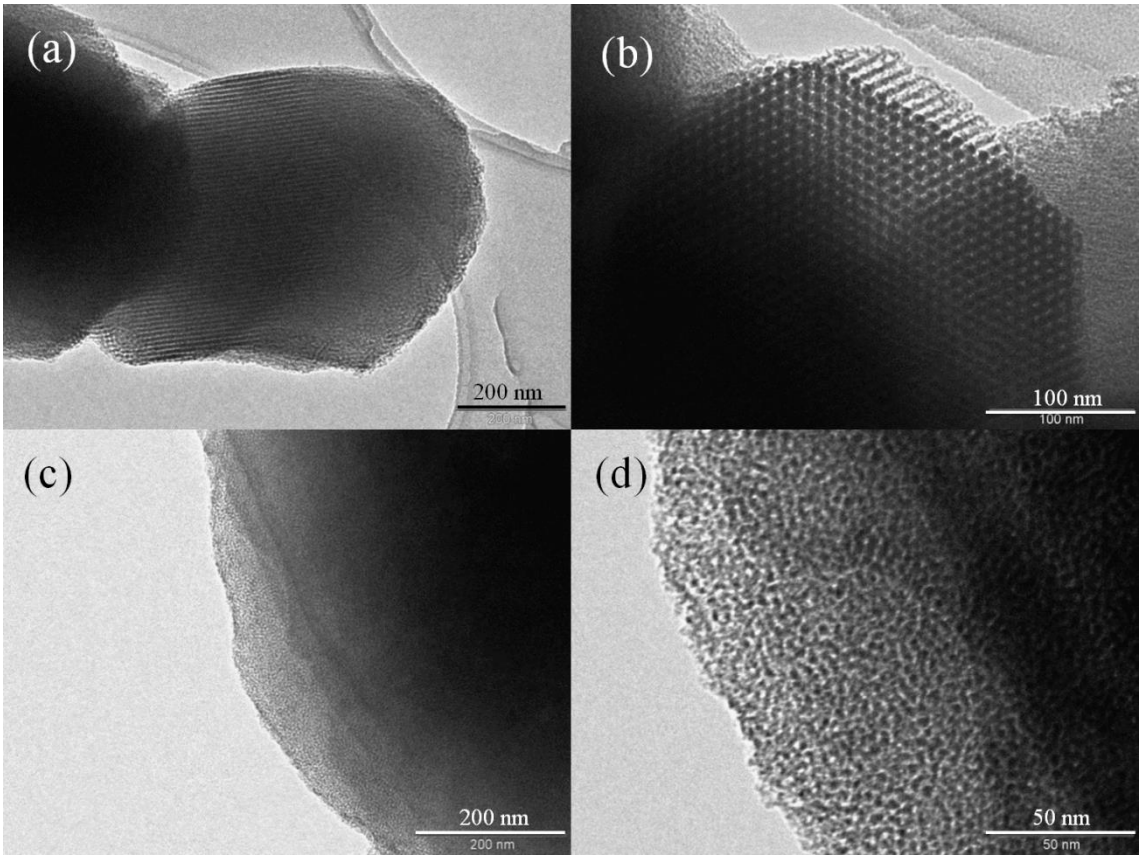

Figure 6. TEM images of Pd-functionalized materials (a) SBA-15-Pd-20 and (b) MSU-2-Pd-5

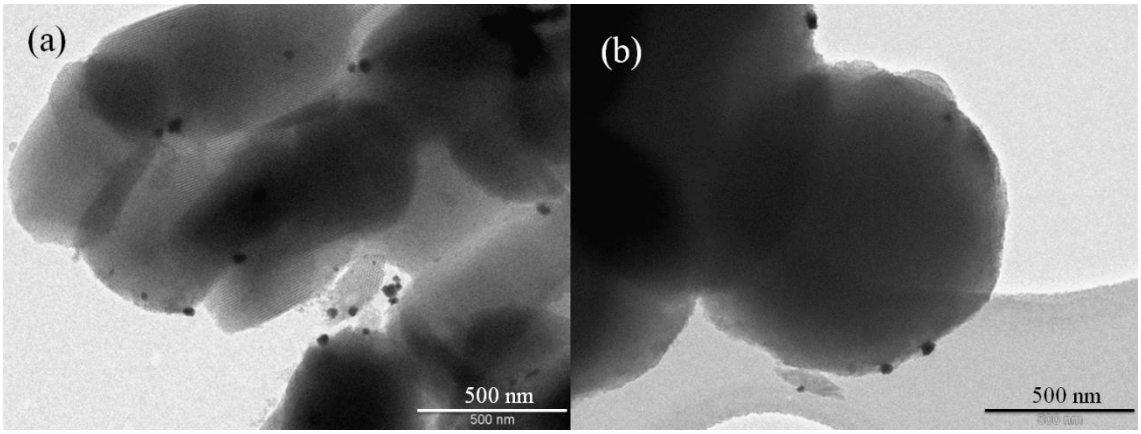

Figure 7. TEM images of Pd-functionalized materials (a) **SBA-15-Pd-20** and (b) **MSU-2-Pd-15** after 6 h of reaction.

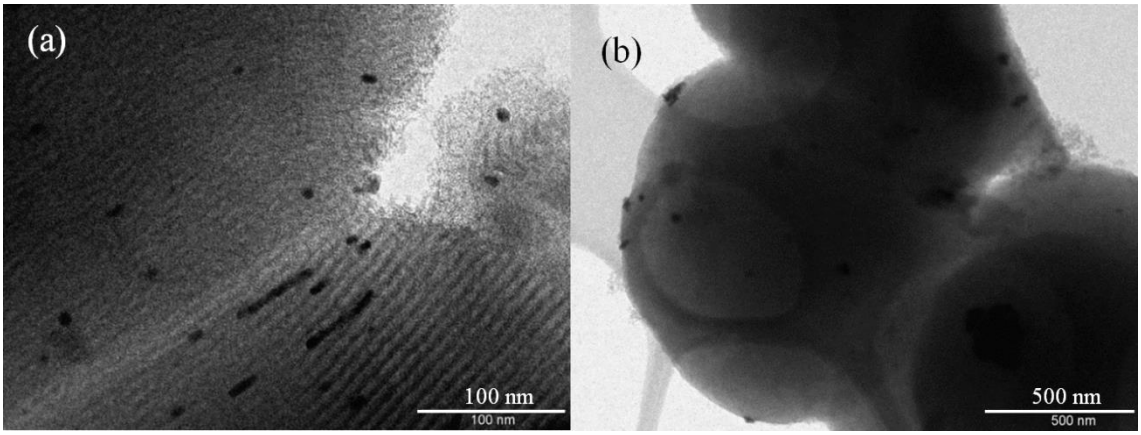

Figure 8. Results of the recyclability tests using the catalysts **SBA-15-Pd-50** and **MSU-2-Pd-15**

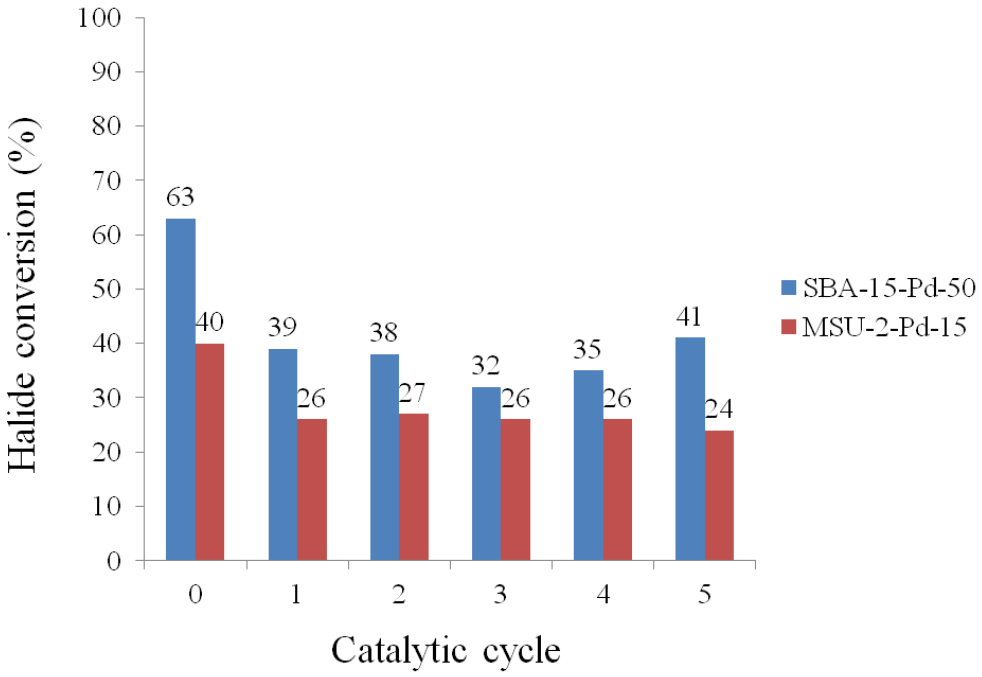

Figure 9. Cell survival vs. material concentration for different cancer cell lines (96 h).

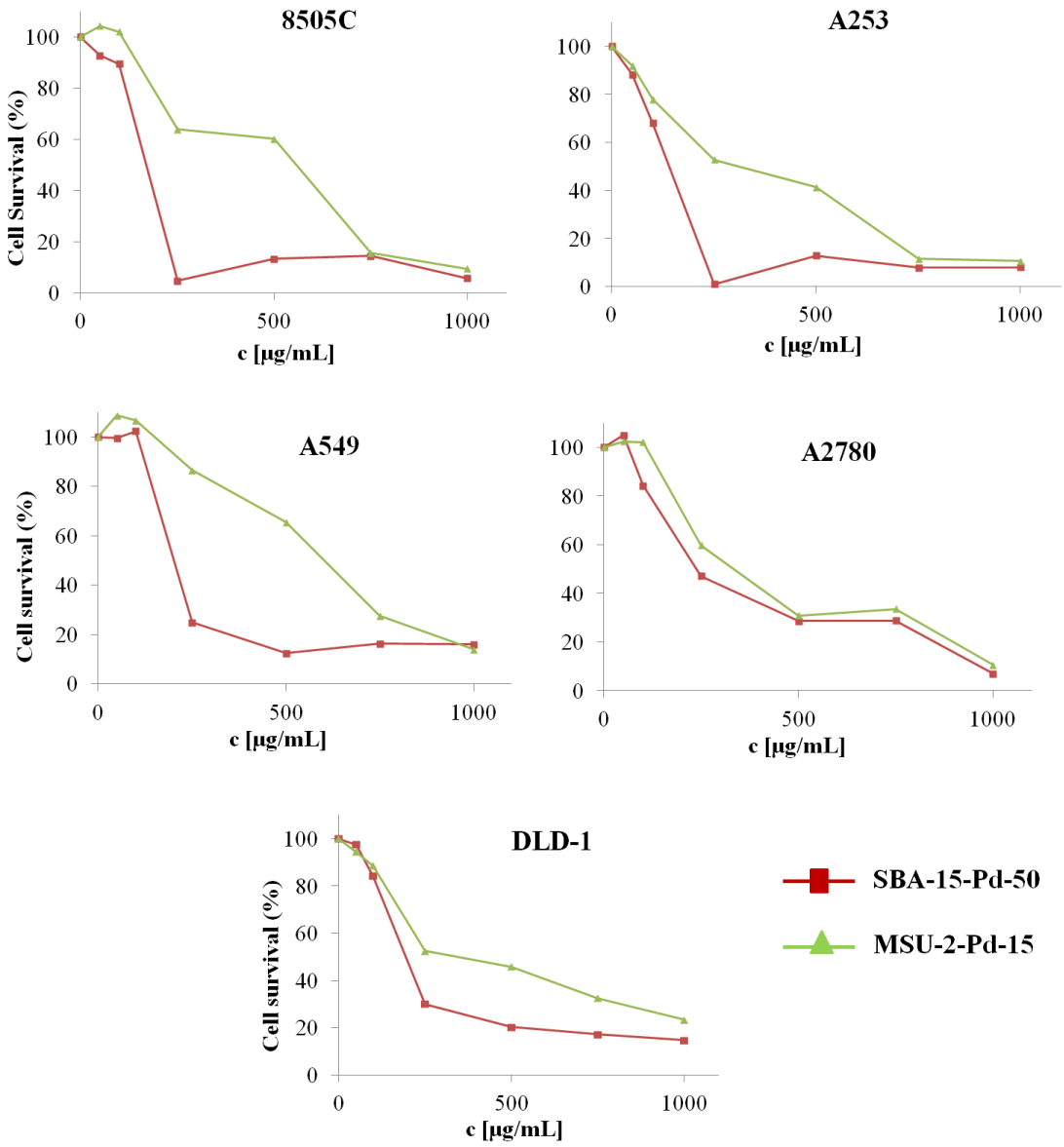

Scheme 1

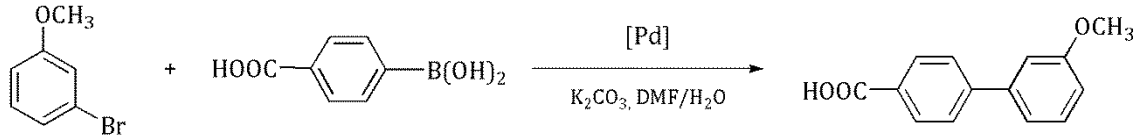

Scheme 2

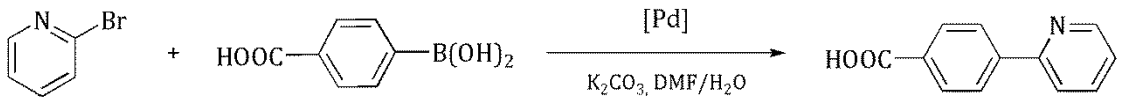

Table 1. [$PdCl_2$(cod)] quantities and Pd loading of the functionalization reactions Palladium loading on SBA-15 and MSU-2

Material	Starting Material (2.0 g)	Theoretical Pd content (%)	Pd (mg)	[$PdCl_2$(cod)] (mg)	Experimental Pd content (%)
SBA-15-Pd-1	SBA-15	1	20	54	0.39
SBA-15-Pd-2	SBA-15	2	40	108	0.54
SBA-15-Pd-5	SBA-15	5	101	270	1.20
SBA-15-Pd-10	SBA-15	10	201	540	2.10
SBA-15-Pd-20	SBA-15	20	388	1040	6.11
SBA-15-Pd-50	SBA-15	50	1006	2700	12.80
MSU-2-Pd-1	MSU-2	1	20	54	0.63
MSU-2-Pd-2	MSU-2	2	40	108	0.48
MSU-2-Pd-5	MSU-2	5	101	270	0.70
MSU-2-Pd-10	MSU-2	10	201	540	1.12
MSU-2-Pd-15	MSU-2	15	294	790	2.18
MSU-2-Pd-20	MSU-2	20	388	1040	4.46

Table 2. Specific surface area, average pore diameter and pore volume of all synthesized materials

Material	Specific surface area (m^2/g)	Pore size (Å)	Pore volumen (cm^3/g)
SBA-15	931	53.7	0.851
SBA-15-Pd-1	785	55.9	0.785
SBA-15-Pd-2	751	55.5	0.737
SBA-15-Pd-5	763	54.8	0.738
SBA-15-Pd-10	768	54.8	0.755
SBA-15-Pd-20	714	55.4	0.708
SBA-15-Pd-50	564	58.0	0.809
MSU-2	1052	31.2	1.055
MSU-2-Pd-1	970	32.5	0.990
MSU-2-Pd-2	863	30.8	0.874
MSU-2-Pd-5	979	32.3	0.989
MSU-2-Pd-10	896	31.6	0.901
MSU-2-Pd-15	934	32.2	0.943
MSU-2-Pd-20	919	31.7	0.936

Table 3. Data for the catalytic reactions 1-4 between 3-bromoanisole and 4-carboxyphenylboronic acid

Catalytic test	Catalyst	Temperature (ºC)	Br conversión (%)	Br conversion per Pd mg (%)
1	**SBA-15-Pd-20**	110	45±1	14.7±0.4
2	**SBA-15-Pd-20**	70	51±2	16.7±0.7
3	**SBA-15-Pd-5**	110	15±1	25.0±1.7
4	**SBA-15-Pd-5**	70	29±1	48.3±1.7
5	**MSU-2-Pd-20**	110	17±2	7.6±0.9
6	**MSU-2-Pd-20**	70	19±2	8.5±0.9
7	**MSU-2-Pd-5**	110	12±2	34.3±7.0
8	**MSU-2-Pd-5**	70	15±1	42.9±3.5
9	**$[Pd(PPh_3)_4]$**	110	84±3	168±6
10	**$[Pd(PPh_3)_4]$**	70	92±1	184±2

Table 4. Data for the catalytic reactions 1-4 between 2-bromopyridine and 4-carboxyphenylboronic acid

Catalytic test	Catalyst	Temperature (°C)	Br conversion (%)	Br conversion per Pd mg (%)
11	**SBA-15-Pd-20**	110	17±2	5.6±0.7
12	**SBA-15-Pd-20**	70	33±3	10.8±1.0
13	**SBA-15-Pd-5**	110	11±1	18.3±1.7
14	**SBA-15-Pd-5**	70	24±2	40.0±3.4
15	**MSU-2-Pd-20**	110	10±1	4.5±0.5
16	**MSU-2-Pd-20**	70	28±1	12.6±0.5
17	**MSU-2-Pd-5**	110	7±1	20.0±2.9
18	**MSU-2-Pd-5**	70	14±2	40.0±5.8
19	**$[Pd(PPh_3)_4]$**	110	40±1	80±2
20	**$[Pd(PPh_3)_4]$**	70	63±2	126±4

Table 5. Data for the catalytic reactions between 3-bomoanisole and 4-carboxyphenylboronic acid using different catalyst quantities at 70 °C

Catalytic test	Catalyst	Catalyst mass (mg)	Br conversion (%)	Br conversion per Pd mg (%)
21	**SBA-15-Pd-50**	15	66±1	5.2±0.1
22	**SBA-15-Pd-50**	5	27±2	2.1±0.2
23	**MSU-2-Pd-15**	15	39±1	17.9±0.5
24	**MSU-2-Pd-15**	5	5±1	2.3±0.5

Table 6. M_{50} values (μg/mL) of the studied materials (96 h) against the studied cancer cell lines.

Cell line	**SBA-15-Pd-50**	**MSU-2-Pd-15**
8505C	111 ± 20	417 ± 26
A253	110 ± 16	284 ± 14
A549	239 ± 20	553 ± 13
A2780	207 ± 21	257 ± 15
DLD-1	155 ± 6	241 ± 18